The amide I spectrum of parallel β-sheet proteins

Cesare M. Baronio, Huimin Li, Guangyuan Song, Henry Thomas Pigott Annecke, Robert Gustafsson, Markel Martínez-Carranza, Pål Stenmark, Andreas Barth

Department of Biochemistry and Biophysics, Stockholm University

Summary
The amide I absorption of the polypeptide backbone has long been used to analyze the secondary structure of proteins. This approach has gained additional attention in the context of amyloid diseases where a particular focus is on the distinction between parallel and antiparallel β-sheets because these structures often discriminate between pre-fibrillar structures and fibrils. Some earlier infrared spectra with typical features of antiparallel β-sheets were interpreted as arising from the parallel β-sheets of fibrils. Therefore, the ability of infrared spectroscopy to distinguish between both types of β-sheets is debated. While it is established that regular, antiparallel β-sheets give rise to a high wavenumber band near 1690 cm^{-1}, it is less clear whether or not this band may also occur for parallel β-sheets. Here we present and analyze the amide I spectra of two β-helix proteins, SV2 and Pent. The overall shape of the proteins is that of a cuboid which has parallel β-sheets on its four sides, which are connected by bends. The main features of their amide I spectrum are a band at 1665, and two bands between 1645 and 1628 cm^{-1}. Both proteins exhibit also a weak component band near 1690 cm^{-1}. Calculations of the amide I spectrum indicate that the absorption at high wavenumbers is not caused by the parallel β-sheets but by the bends between the β-strands. We therefore suggest to modify the interpretation of the amide I spectrum as follows: a high wavenumber band near 1690 cm^{-1} may be caused by other structures than antiparallel β-sheets. However, when the spectrum consists of only two distinct bands, one near 1690 cm^{-1} and one near 1630 cm^{-1}, then an assignment to antiparallel β-sheets is consistent with the literature.

β-sheets are a main structural component of proteins. They are also prominent in the misfolded forms of proteins that are involved in amyloidoses.[1,2] A prominent example for the latter is Alzheimer's disease, which is the most common neurodegeneration.[3] Amyloidoses are characterized by the formation of amyloid fibers which consist of β-strands that run perpendicular to the fiber axis. The orientation of adjacent strands is parallel in most cases, but antiparallel β-sheets have also been observed.[4–6] Amyloids form from unstructured or destabilized protein monomers in a complicated aggregation process[7,8] that involves a great number of intermediate, smaller aggregates.[5,9–11] Interestingly, these aggregates seem to have a different β-sheet architecture than the fibrils.[12,13] For example, the amyloid-β (Aβ) peptide that constitutes the amyloid fibers in Alzheimer's disease forms oligomers with antiparallel β-sheets but its fibers have parallel β-sheets.
The general interest in proteins and the need to achieve a mechanistic, molecular understanding of amyloidoses ask for simple and rapid methods to distinguish parallel and antiparallel β-sheets. Infrared spectroscopy has long been suggested to be one of such tools. It has been used for decades to analyze the secondary structure analysis of proteins[14–18] by exploiting the conformational sensitivity of the absorption of the amide I vibration. This vibration involves mainly the carbonyl stretching vibration of the peptide backbone. The vibrations of individual amide groups couple electrostatically through space giving rise to delocalized normal modes, each of which involves several amide groups - typically up to around ten.[19–25] A band at the high wavenumber end of the amide I spectrum has been assigned to antiparallel β-sheets from experimental data and computations. It has been debated however whether parallel β-sheets also can generate such a band, for two reasons: (i) Early work on Aβ has observed a high wavenumber band and concluded that the fibrils consist of antiparallel β-sheets.[13] Later, solid state nuclear magnetic resonance work corrected this interpretation and demonstrated the parallel arrangement of the β-strands in Aβ fibrils. (ii) Spectra of some proteins that are largely composed of parallel β-sheets also show this band.[26,27] Thus, the use of the high wavenumber band as a marker band for antiparallel β-sheets is controversial and further work is required to clarify the situation.

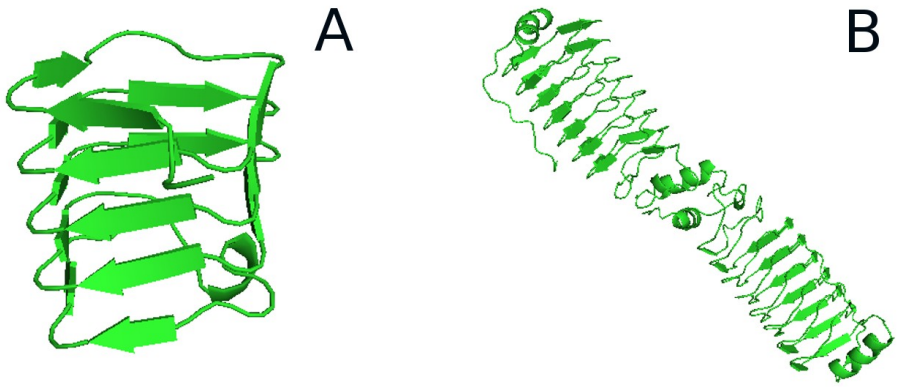

Figure 1: structures of SV2 (panel A), as extract of PDB entry 6ES1, and Pent (panel B), using chain A and B of PDB entry 6FLS.

This study reinvestigates the assignment of the high wavenumber band by studying two β-helix proteins in experiments and calculations. The structure of these proteins - SV2[28–30] and Pent - is shown in Fig. 1. In these proteins the β-helix is composed by a string of squared coils, each one of them is created by the arrangement of four pentapeptide repeats. Each monomer in Pent has eight coils, whereas SV2 has five coils. We show that the proteins exhibit a weak high wavenumber band

which is caused by the 90°-bends between the parallel β-sheets. Based on these results, we suggest guidelines for the interpretation of high wavenumber bands in amide I spectra of proteins.

Materials and Methods

Experiments

The proteins SV2 and Pent were expressed and purified according to previously published protocols.[29,30] The proteins were stored at concentrations of 8 mg/mL (SV2) and 11 mg/mL (Pent) at -80°C in 20 mM HEPES pH 7.5, 300 mM NaCl, 10% glycerol, and 2mM tris(2-carboxyethyl)phosphine (SV2) or 2 mM Trichloroethene (Pent). For spectroscopy, the proteins were studied in the original buffer (Pent) or after buffer exchange using 3kDa Amicon centrifugal filters and a Jouan A14 centrifuge at 14000 rpm. The buffer was exchanged three times for 20-30 min at 4% of the original SV2 concentration. Filtration was performed at room temperature to avoid aggregation at low temperatures. The recovered protein sample had approximately the same volume, so that the final protein concentration was approximately the same as the starting concentration of 8 mg/mL. The solvent was $^{1}H_2O$ for all experiments.

The sample was placed between two BaF_2 or CaF_2 windows, one of which had a through of ~6 μm depth which determined the optical pathlength. The outer contact area of the windows was covered with vacuum grease to avoid sample loss.

Spectra were recorded with a Bruker Tensor 37 Fourier transform infrared spectrometer (Bruker, Ettlingen, Germany) at a spectral resolution of 2 cm^{-1}. 50 interferograms were averaged for each sample and background spectrum, apodized with a Blackman Harris 3-term function and zero-filled with a factor of 2. 20 of such spectra were averaged for each sample. Two (SV2) or four (Pent) samples were prepared and their spectra averaged. The samples were measured using a sample shuttle (Bruker) that allowed to record background and sample spectrum in succession without opening the sample chamber. A metal grid was placed in the background position so that the light intensity of the background spectrum approximately matched the light intensity of the sample spectrum. For half of the Pent samples, a Ge filter and a 25 μm cellulose film blocked the light above 2200 cm^{-1} and below 1400 cm^{-1}. These three measures allowed us to increase the aperture to either 1.5 mm (grid only) 3 mm (grid, Ge filter, and cellulose) for a better signal to noise ratio[31]. The spectrometer was continuously purged with dry air. Second derivatives were calculated with the OPUS 5.5 software and a smoothing range of 17 points.

Calculations

The calculations were based on two different PDB entries: we used an extract of PDB entry 6ES1[29] for SV2 and chain A and B of PDB entry 6FLS[30] for Pent.

The simulated amide I spectra were calculated from mass-normalized force constants matrices using a Matlab program.[32] A mass-normalized diagonal force constant of 1.7128 mdyn $Å^{-1}$ u^{-1}, corresponding to a 1705 cm^{-1}, was assigned to each amide group of Pent and SV2. The diagonal elements of the mass-normalized force constants matrices were then modified according to (i) the local environment effect,[33] (ii) the effect of inter-amide hydrogen bond using a model suggested by Ge and coworkers[34] and (iii) solvation effects based on the solvent accessible surface.[32]

The coupling constants were obtained from density functional theory calculations for nearest neighbor interactions[33] and calculated from transition dipole coupling for other interactions. The parameters for the transition dipole moment used for the calculation of the transition dipole coupling constants were previously optimized.[35] The magnitude of the dipole derivative was fixed to 2.20 D $Å^{-1}$ $u^{-1/2}$, the angle was fixed to 22° and *A*, the parameter that describes the effect of hydrogen bonding on the magnitude of the dipole derivative, was fixed to 0.01 cm. The position of the transition dipole moment was located at 1.043 Å from the C-atom along the C=O bond and at 0.513 Å along the C-N bond.

We analyzed the contributions of amide groups to the intensity of the spectrum both for SV2 and Pent. The contributions were calculated by squaring the amplitude of each amide group in each normal mode and by multiplying it with the intensity of the normal mode. Each amide group was assigned to the secondary structure of the residue containing the carbonyl group (see below) and the contributions of the considered secondary structure types were added. This gave the intensity contributions of the different secondary structures to each normal mode. We then combined the contributions of all normal modes within a 5 cm^{-1} interval.
For secondary structure classification we used the automatic assignment made in PyMol for α-helix and β-sheet. Amide groups of residues that were not classified by PyMol were assigned manually as described in the following. The category "Beta bend" is related to the bends between two β-strands; the category "other bend" is related to the amide groups of the bends between a β-strand and other secondary structure found at the edges of the cuboid protein structures; and the new category "other" contained the amide groups without any secondary structure assignment and not located in any type of bend.

Results

We measured the infrared absorbance spectrum of the two β-helix proteins SV2 and Pent. Our focus is on the amide I band of protein absorption (1700-1600 cm^{-1}), which sensitive to protein backbone conformation. It usually contains several component bands, which are hard to discriminate in the broad absorbance spectrum. In order to reveal the component bands better, we used the second derivative of absorbance, in which the component bands show up as negative bands. Fig. 2 (black line) shows the experimental second derivative spectrum of SV2 and Fig. 3 (black line) the respective spectrum of Pent.
The SV2 spectrum (Fig. 2) has two minima in the amide I range, one at 1669 cm^{-1} and one at 1636 cm^{-1}. Both of them reveal a substructure: The main band at 1636 cm^{-1} has a shoulder on its high wavenumber side near 1647 cm^{-1} and the 1669 cm^{-1} band is unusually broad, indicating that it consists of two unresolved bands. In the high wavenumber region, which is of prime interest in this study, the second derivative shows a small inflection which indicates a small component band near 1690 cm^{-1}.
The Pent spectrum (Fig. 3) has three prominent bands at 1664, 1642, and 1629 cm^{-1}. It also has a high wavenumber band at 1691 cm^{-1} that seems to consist of two components and which is more prominent than that of SV2.
The band near 1690 cm^{-1} of both proteins appears in the spectral range that is characteristic of the high wavenumber component of antiparallel β-sheets. However, these proteins do not contain this secondary structure, making such an assignment impossible. In order to reveal the origin of this band, we calculated the amide I spectrum with our in-house Matlab program[32] using optimized parameters for the transition dipole moment (TDM).[35] The such calculated spectra are compared to the experimental spectra in Figs. 2 and 3.
Figs. 2 and 3 show also the simulated second derivatives for SV2 and Pent, respectively, as red lines. A good agreement of the band positions is generally reached for both the proteins. For SV2, the bands at 1669 cm^{-1} and 1690 cm^{-1} are matched, whereas the experimental main band at 1636 cm^{-1} and its shoulder at 1647 cm^{-1} are located respectively at 1625 cm^{-1} and 1645 cm^{-1} in the simulation. For Pent, the bands at 1691 cm^{-1}, 1664 cm^{-1} and 1629 cm^{-1} are matched, whereas the experimental band at 1642 cm^{-1} is shifted to 1650 cm^{-1} in the simulation.
The intensities of the experimental and simulated second derivatives are not always matched. The experimental intensities of the second derivatives for the bands in the central region of the plotted spectrum (1680-1640 cm^{-1}) are quite respected. However, the simulated bands at 1690 cm^{-1}, 1630 cm^{-1} (for Pent) and 1625 cm^{-1} (for SV2) showed much more prominent intensities than the corresponding experimental bands. We note that second derivatives are very sensitive to the band width of the component bands in the absorbance spectrum. Narrow bands cause strong bands in the second derivatives while broad bands generate much smaller bands. Therefore, small deficiencies in the simulations may lead to rather large deviations of the simulated second derivative amplitudes

from the experimental ones. These deficiencies could be caused by either too small or too large wavenumber deviations of close-lying normal modes, a deficiency of the calculation of the intrinsic wavenumbers of local amide I oscillators, and the neglect of dynamics.

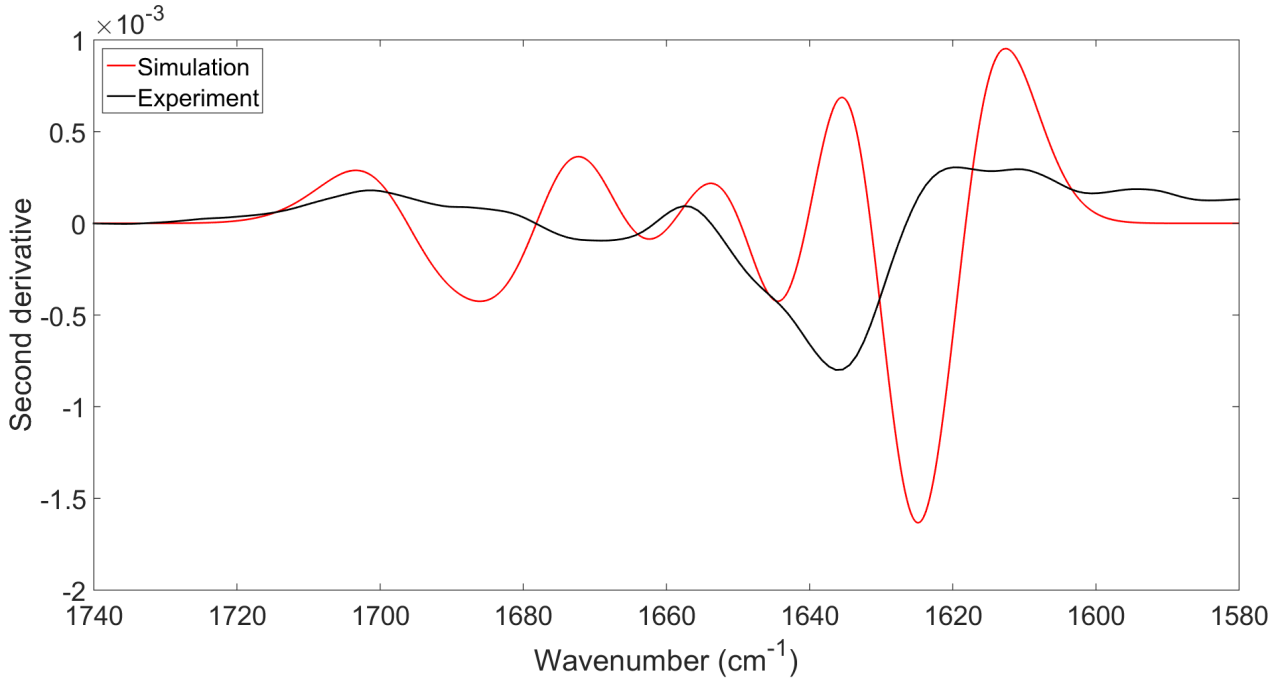

Figure 2: experimental (black) and simulated (red) second derivative of IR absorbance for SV2

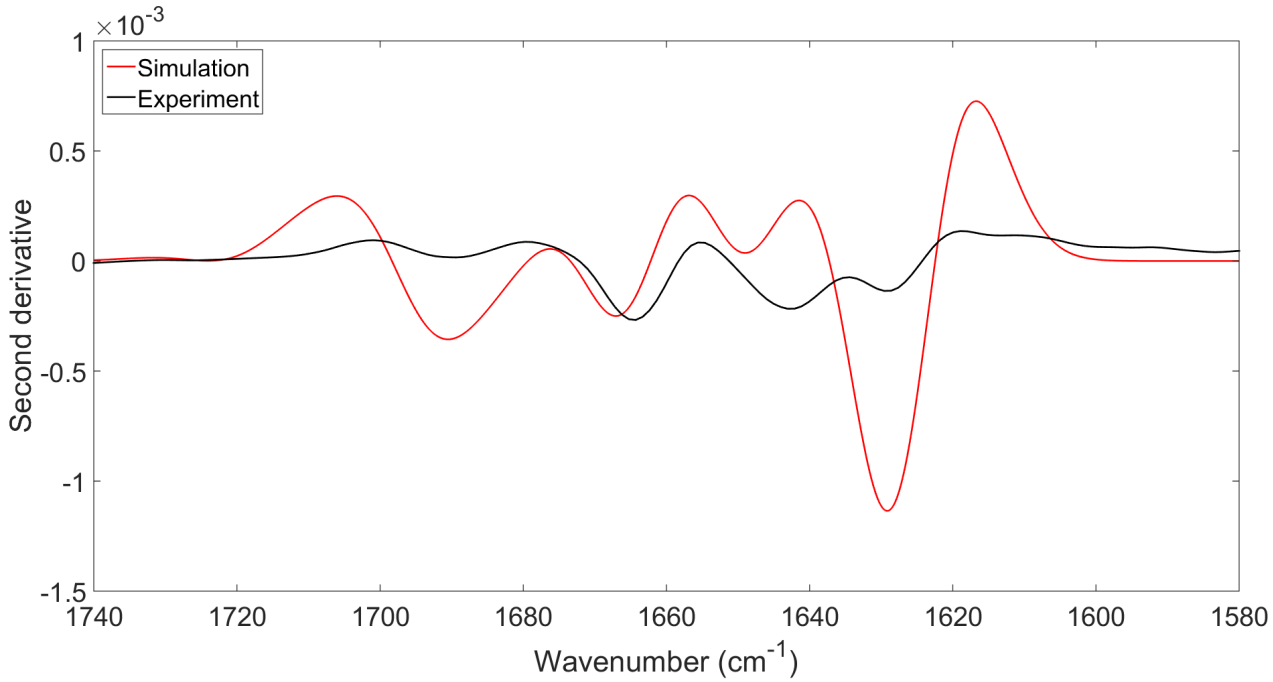

Figure 3: experimental (black) and simulated (red) second derivative of IR absorbance for Pent

We then analyzed the contributions of different secondary structure categories to the intensities of the spectrum both for SV2 and Pent, represented respectively in Figs. 4 and 5. The main contribution of the β-sheets is located at low wavenumbers, between 1640 cm^{-1} and 1620 cm^{-1}. It decreases with increasing wavenumber, with a slightly increase at 1690 cm^{-1}. The contributions related to α-helix is calculated at wavenumbers higher than 1655 cm^{-1}. This is clearly seen in for Pent, where the number of α-helical amide groups is higher than in SV2. The contribution of β-

bends can be found in wavenumbers higher than 1665 cm^{-1} and is largest in the interval between 1685 cm^{-1} and 1695 cm^{-1}. The main contribution of the other bends is located in the same interval as that of the β-bends. Due to a high number of these bends in Pent, small contributions can also be found in the β-sheet region, between 1660 cm^{-1} and 1630 cm^{-1}. The other amide groups generally contributes throughout the entire amide I spectrum.
If we focus our attention on the interval between 1695 cm^{-1} and 1685 cm^{-1}, where the high wavenumber band is located, we can notice that the contribution of β-sheets is limited. All the other secondary structures contribute to this band for Pent, whereas the two types of bend are the responsible of this band for SV2.

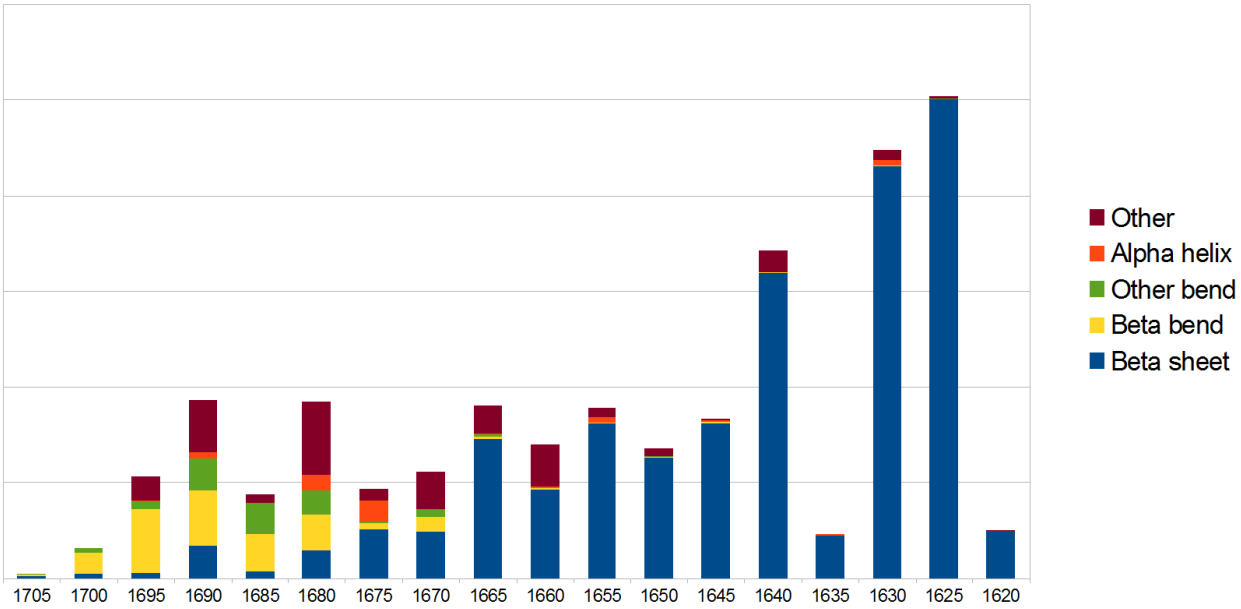

Figure 4: residue contribution analysis for SV2. See text for the explanation of the categories of the secondary structures.

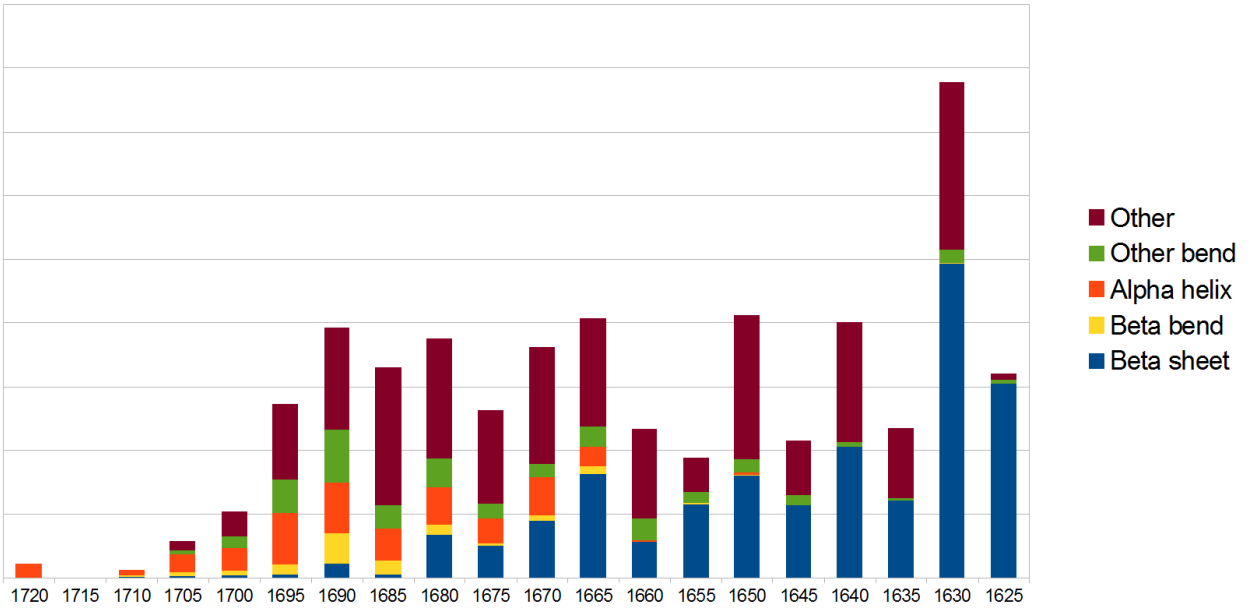

Figure 5: residue contribution analysis for Pent. See text for the explanation of the categories of the secondary structures.

Discussion

A high wavenumber band near 1695 cm^{-1} in $^{1}H_2O$ or 1685 cm^{-1} in $^{2}H_2O$ is often considered a marker band for antiparallel β-sheets. It is commonly observed for proteins with antiparallel β-sheets[36,37] and is expected from calculations as long as the sheets are sufficiently extended and planar.[38–40] Calculations do not predict this band for parallel β–sheets[39–41] and a distinct high wavenumber shoulder is not observed for peptides designed or shown to form parallel β-sheets.[42–44] It is neither present in spectra of fibrils of several amyloid proteins that consist of parallel β-sheets[13] or a parallel β-sheet protein[45], although there is an absorbance tail in the high wavenumber region of the amide I spectrum.

Site-specific labeling can also yield information about the organization of β-sheets. Relatively strong intensity of the ^{13}C-band and a spectral position close to that in a ^{12}C-environment are indicative of antiparallel β-sheets.[46–54] Such properties of the ^{13}C-band correlate with the appearance of a high wavenumber shoulder in the spectrum of the unlabeled peptides. The correlation holds even for Aβ variants that convert from antiparallel to parallel β-sheet structure.[47,55] Nevertheless, spectra with such correlated features have occasionally been assigned to parallel β-sheets.[56,57] In these cases, the results of site-specific labeling do not agree with those expected for aligned parallel β-sheets so the parallel orientation of adjacent strands is not established without doubt. The spectral properties were explained by assuming some distance between the labeled residues[56] and by assigning the high wavenumber band to loops[57] which is in agreement with the present study.

However, there are previous experimental studies of parallel β-sheet proteins which observe high wavenumber bands. Of the two proteins flavodoxin and triosephosphate isomerase, the latter shows distinct bands above 1680 cm^{-1} in second derivate spectra of deuterated proteins. Also two of three β-helix proteins (H-form) exhibited a second derivative band above 1690 cm^{-1}, one of which was very distinct.[27] This is confirmed by our present study of SV2 and Pent which show a high wavenumber band to different degrees. For SV2, this band is hard to detect and would therefore not qualify as a marker band for antiparallel β-sheets. Instead, our SV2 spectrum agrees with the cited calculations and model studies which indicate that parallel β-sheets do not produce such a band. On the other hand, the Pent spectrum shows a clear high wavenumber band which would be assigned to antiparallel β-sheets according to the literature. As this protein does not contain antiparallel β-

sheets, such an assignment is not an option. We therefore explored in calculations the structural reason for its appearance.
The simulations reproduced well the experimental band positions in the second derivatives of absorbance, but not the intensities. The secondary structure contributions to the amide I band are in accordance with previous calculations. Torii and Tasumi[58] calculated the main absorption band for the parallel β-sheets at 1630 cm^{-1}, with smaller bands between 1680 cm^{-1} and 1650 cm^{-1}; these results are in agreement with our calculated contribution of the parallel β-sheets (1640-1625 cm^{-1} for the main contribution and smaller contributions between 1680 cm^{-1} and 1640 cm^{-1}).
In the same work,[58] the main band of α-helices was located at 1640 cm^{-1}, three small bands at 1660 cm^{-1}, 1670 cm^{-1} and close to 1680 cm^{-1}. Our calculated contributions shows instead a spread contribution between 1660 cm^{-1} and 1700 cm^{-1}, which extends until 1720 cm^{-1} for Pent.
Turns have been calculated to absorb in the region between 1700 cm^{-1} and 1630 cm^{-1} depending on the dihedral angles.[59–61] In our calculations, much of the absorption of bends is found at high wavenumbers, which is in line to the assignments for a fiber model of the human islet amyloid polypeptide.[57] According to this study, stacking of turn structures increased the spectral range that is covered by turn vibrations. Thus, the coupling between the vibrations in adjacent bends with similar conformation can increase the maximum wavenumber and decrease the minimum wavenumber of the bend normal modes.
Amide groups that cannot be considered as α-helix and β-sheets can absorb throughout the entire amide I region.[58] Our calculated contributions for bends and "other amide groups" confirm that.

Conclusions

There is no doubt that extended antiparallel β-sheets give rise to a high wavenumber band (above 1690 cm^{-1} in ^1H_2O and above 1680 cm^{-1} in ^2H_2O). However, other secondary structures may also contribute in this spectral range. Therefore, the observation of a high wavenumber band alone cannot be taken as evidence for the presence of antiparallel β-sheets. We suggest that the remainder of the amide I spectrum also needs to be taken into account. In the cases where proteins without antiparallel β-sheets produce a high wavenumber band, Pent in this study and several other β-helix proteins in the study by Khurana and Fink,[27] they also show prominent bands outside the region of β-sheet absorption, in our case at 1665 cm^{-1}. When this is the case, a high wavenumber band should not be used as a marker of antiparallel β-sheets. However, when the only distinct bands are in the main β-sheet region (< 1640 cm^{-1}) and above 1690 cm^{-1} (1680 cm^{-1} in ^2H_2O), then the high wavenumber band indicates the presence of antiparallel β-sheets. The rationale for this assignment is that non-β-sheet structures, which do absorb at high wavenumbers, do not cause a strong band below 1640 cm^{-1}. Such spectra are for example observed for oligomers of Aβ,[62,63] which therefore consist of antiparallel β-sheets.

Acknowledgements

We gratefully acknowledge funding from Stockholm regional council for salaries and from Knut and Alice Wallenberg foundation for the spectrometer.

References

1 J. Johansson, L. Olson, J. Andersson, G. Johansson and B. Winblad, *J. Intern. Med.*, 2016, **280**, 136–138.

2 T. P. J. Knowles, M. Vendruscolo and C. M. Dobson, *Nat. Rev. Mol. Cell Biol.*, 2014, **15**, 384–396.

3 C. M. Dobson, *Rend. Lincei*, 2015, **26**, 251–262.

4 D. S. Eisenberg and M. R. Sawaya, *Annu. Rev. Biochem.*, 2017, **86**, 69–95.

5 F. Chiti and C. M. Dobson, *Annu. Rev. Biochem.*, 2017, **86**, 27–68.

6 R. Riek, *Cold Spring Harb. Perspect. Biol.*, 2017, **9**, a023572.

7 M. Törnquist, T. C. T. Michaels, K. Sanagavarapu, X. Yang, G. Meisl, S. I. A. Cohen, T. P. J. Knowles and S. Linse, *Chem. Commun.*, 2018, **54**, 8667–8684.

8 T. C. T. Michaels, A. Šarić, J. Habchi, S. Chia, G. Meisl, M. Vendruscolo, C. M. Dobson and T. P. J. Knowles, *Annu. Rev. Phys. Chem.*, 2018, **69**, 273–298.

9 I. Benilova, E. Karran and B. De Strooper, *Nat. Neurosci.*, 2012, **15**, 349–57.

10 K. L. Viola and W. L. Klein, *Acta Neuropathol.*, 2015, **129**, 183–206.

11 E. N. Cline, M. A. Bicca, K. L. Viola and W. L. Klein, *J. Alzheimer's Dis.*, 2018, **64**, S567–S610.

12 R. Aleksis, F. Oleskovs, K. Jaudzems, J. Pahnke and H. Biverstål, *Biochimie*, 2017, **140**, 176–192.

13 R. Sarroukh, E. Goormaghtigh, J.-M. Ruysschaert and V. Raussens, *Biochim. Biophys. Acta - Biomembr.*, 2013, **1828**, 2328–2338.

14 D. M. Byler and H. Susi, *Biopolymers*, 1986, **25**, 469–487.

15 E. Goormaghtigh, V. Cabiaux and J. M. Ruysschaert, *Subcell. Biochem.*, 1994, **23**, 405–50.

16 J. L. R. Arrondo, A. Muga, J. Castresana and F. M. Goñi, *Prog. Biophys. Mol. Biol.*, 1993, **59**, 23–56.

17 M. Jackson and H. H. Mantsch, *Crit. Rev. Biochem. Mol. Biol.*, 1995, **30**, 95–120.

18 H. Fabian and W. Mäntele, in *Handbook of vibrational spectroscopy*, eds. J. M. Chalmers and P. Griffiths, John Wiley & Sons, Chichester, 2002, pp. 3399–3426.

19 E. B. Dunkelberger, M. Grechko and M. T. Zanni, *J. Phys. Chem. B*, 2015, **119**, 14065–14075.

20 S. Woutersen and P. Hamm, *J. Chem. Phys.*, 2001, **115**, 7737–7743.

21 P. Hamm, M. Lim and R. M. Hochstrasser, *J. Phys. Chem. B*, 1998, **102**, 6123–6138.

22 S. Ham, S. Hahn, C. Lee, T.-K. Kim, K. Kwak and M. Cho, *J. Phys. Chem. B*, 2004, **108**, 9333–9345.

23 S. Hahn, S. Ham and M. Cho, *J. Phys. Chem.*, 2005, **109**, 11789–11801.

24 J.-H. Choi, S. Hahn and M. Cho, *Biopolymers*, 2006, **83**, 519–536.

25 J.-H. Choi, H. Lee, K.-K. Lee, S. Hahn and M. Cho, *J. Chem. Phys.*, 2007, **126**, 045102.

26 H. Susi and D. M. Byler, *Arch. Biochem. Biophys.*, 1987, **258**, 465–469.

27 R. Khurana and A. L. Fink, *Biophys. J.*, 2000, **78**, 994–1000.

28 R. M. Benoit, D. Frey, M. Hilbert, J. T. Kevenaar, M. M. Wieser, C. U. Stirnimann, D. McMillan, T. Ceska, F. Lebon, R. Jaussi, M. O. Steinmetz, G. F. X. Schertler, C. C. Hoogenraad, G. Capitani and R. A. Kammerer, *Nature*, 2014, **505**, 108–111.

29 R. Gustafsson, S. Zhang, G. Masuyer, M. Dong and P. Stenmark, *Toxins (Basel).*, 2018, **10**, 153.

30 L. Notari, M. Martínez-Carranza, J. A. Farías-Rico, P. Stenmark and G. von Heijne, *J. Mol. Biol.*, 2018, **430**, 5196–5206.

31 M. Baldassarre and A. Barth, *Analyst*, 2014, **139**, 5393–9.

32 E.-L. E.-L. Karjalainen, T. Ersmark and A. Barth, *J. Phys. Chem. B*, 2012, **116**, 4831−4842.

33 R. D. Gorbunov, D. S. Kosov and G. Stock, *J. Chem. Phys.*, 2005, **122**, 224904.

34 H. Maekawa, C. Toniolo, Q. B. Broxterman and N. Ge, 2007, 3222–3235.

35 C. M. Baronio and A. Barth, *J. Phys. Chem. B*, 2020, acs.jpcb.9b11793.

36 Y. N. Chirgadze, B. V Shestopalov and S. Y. Venyaminov, *Biopolymers*, 1973, **12**, 1337–1351.

37 S. Y. Venyaminov and N. N. Kalnin, *Biopolymers*, 1990, **30**, 1259–1271.

38 Y. N. Chirgadze and N. A. Nevskaya, *Biopolymers*, 1976, **15**, 607–25.

39 J. Kubelka and T. A. Keiderling, *J. Am. Chem. Soc.*, 2001, **123**, 12048–12058.

40 W. R. W. Welch, J. Kubelka and T. A. Keiderling, *J. Phys. Chem. B*, 2013, **117**, 10343–10358.

41 Y. N. Chirgadze and N. A. Nevskaya, *Biopolymers*, 1976, **15**, 627–36.

42 N. Yamada, K. Ariga, M. Naito and K. Matsubara, 1998, **600**, 12192–12199.

43 J. Bandekar and S. Krimm, *Biopolymers*, 1988, **27**, 885–908.

44 P. Chitnumsub, W. R. Fiori, H. A. Lashuel, H. Diaz and J. W. Kelly, *Bioorg. Med. Chem.*, 1999, **7**, 39–59.

45 M. S. Celej, R. Sarroukh, E. Goormaghtigh, G. D. Fidelio, J.-M. Ruysschaert and V. Raussens, *Biochem. J.*, 2012, **443**, 719–726.

46 C. Paul, J. Wang, W. C. Wimley, R. M. Hochstrasser and P. H. Axelsen, *J. Am. Chem. Soc.*, 2004, **126**, 5843–50.

47 F. Xu, Z. Fu, S. Dass, A. E. Kotarba, J. Davis, S. O. Smith and W. E. Van Nostrand, *Nat. Commun.*, 2016, **7**, 13527.

48 W. R. W. Welch, T. A. Keiderling and J. Kubelka, *J. Phys. Chem. B*, 2013, **117**, 10359–69.

49 K. J. Halverson, I. Sucholeiki, T. T. Ashburn and P. T. Lansbury, *J. Am. Chem. Soc.*, 1991, **113**, 6701–6703.

50 S. A. Petty and S. M. Decatur, 2005, 13488–13489.

51 G. Shanmugam and P. L. Polavarapu, *J. Struct. Biol.*, 2011, **176**, 212–9.

52 A. K. Mehta, K. Lu, W. S. Childers, Y. Liang, S. N. Dublin, J. Dong, J. P. Snyder, S. V. Pingali, P. Thiyagarajan and D. G. Lynn, *J. Am. Chem. Soc.*, 2008, **130**, 9829–9835.

53 R. A. G. D. Silva, W. Barber-Armstrong and S. M. Decatur, *J. Am. Chem. Soc.*, 2003, **125**, 13674–13675.

54 J. W. Brauner, C. Dugan and R. Mendelsohn, *J. Am. Chem. Soc.*, 2000, **122**, 677–683.

55 Z. Fu, D. Aucoin, J. Davis, W. E. Van Nostrand and S. O. Smith, *Biochemistry*, 2015, **54**, 4197–4207.

56 C. Paul and P. H. Axelsen, *J. Am. Chem. Soc.*, 2005, **127**, 5754–5.

57 D. B. Strasfeld, Y. L. Ling, R. Gupta, D. P. Raleigh and M. T. Zanni, *Methods*, 2009, 15679–15691.

58 H. Torii and M. Tasumi, *J. Chem. Phys.*, 1992, **96**, 3379–3387.

59 S. Krimm and J. Bandekar, *Biopolymers*, 1980, **19**, 1–29.

60 S. Krimm and J. Bandekar, *Adv. Prot. Chem.*, 1986, **38**, 181–367.

61 P. Lagant, G. Vergoten, G. Fleury and M.-H. Loucheux-Lefebvre, *Eur. J. Biochem.*, 1984, **139**, 149–154.

62 E. Cerf, R. Sarroukh, S. Tamamizu-Kato, L. Breydo, S. Derclaye, Y. F. Dufrêne, V. Narayanaswami, E. Goormaghtigh, J.-M. Ruysschaert and V. Raussens, *Biochem. J.*, 2009, **421**, 415–23.

63 M. Baldassarre, C. M. Baronio, L. A. Morozova-Roche and A. Barth, *Chem. Sci.*, 2017, **8**, 8247–8254.